ACS Combinatorial Science

Research Article

pubs.acs.org/acscombsci

Selection of Chiral Zinc Catalysts for the Kinetic Resolution of Esters via Dynamic Templating

R. Kannappan and K. M. Nicholas*

Department of Chemistry and Biochemistry, Stephenson Life Sciences Research Center, University of Oklahoma, Norman, Oklahoma 73019, United States

Supporting Information

ABSTRACT: Dynamic combinatorial libraries of chiral tetradentate bis-imine zinc(II) complexes have been prepared and screened for (1) their discrimination of enantiomeric picolinate esters and pyridyl phosphonate transition state analogs (TSAs) and (2) their catalytic activity and selectivity for enantioselective methanolysis of racemic picolinate esters. The zinc complexes are in equilibrium with their imine ligands as well as with the aldehyde and amine building blocks that form them, enabling the composition of the library to adapt in response to the introduction of coordinating substrates or TSAs. Binary (L)Zn(OTf)(solv)$^+$ complexes are generated either individually or in libraries from chiral tartrate-derived diamines (**2**,**3**) and a set of *N*-heterocyclic aldehydes (**4**−**12**) and the distribution of complexes established by ESI-MS analysis. Binding studies of the (diimine)Zn(OTf)$_2$ complex libraries with enantiomeric *R*- and *S*-2-pyridyl phosphonate TSA **13** show chiral discrimination via formation of diastereomeric LZn(*R*/*S*-**13**)$^+$ complexes with low to moderate enatioselectivity ratios, k_R/k_S (α), ranging from 0.5 to 5.0; corresponding templating of selected binary complexes with the enantiomeric substrates, PyrCO$_2$CH(OH)Ph (**1**), show negligible chiral recognition. The rate constants for methanolysis of the *R*- and *S*-esters, PyrCO$_2$CH(OH)Ph (**1**) catalyzed by several L*Zn(OTf)$_2$ complexes range in value several fold depending on L and with enantioselectivity ratios, k_R/k_S (α), ranging from 0.76 to 2.8.

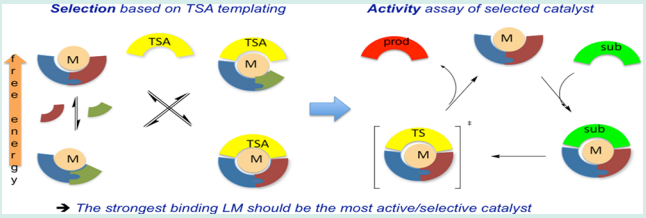

KEYWORDS: *chiral zinc catalysts, esterolysis, dynamic templating, transition state analogs, ESI-MS screening*

INTRODUCTION

In biological systems metalloprotease and -esterase enzymes catalyze the hydrolysis of amides and esters with remarkable efficiency by making use of the protein-ligated metal center to electrophilically activate the substrate and, in some cases, to increase the acidity and the nucleophilicity of coordinated water.[1] For example, carboxypeptidase A and thermolysin are Zn(II)-enzymes that catalyze the hydrolysis of peptides and *O*-acyl derivatives of α-hydroxycarboxylic acids.[2,3] To better understand the factors that control the detailed properties of the active sites of zinc enzymes, numerous model complexes have been investigated.[4] Studies of scorpionate- and other tripodal-Zn complexes have led to the elucidation of key mechanistic features of the catalysis by Zn-enzymes.[5] These include biomimetic hydrolyses as well as the modeling of intermediates of peptidase and carbonic anhydrase catalytic cycles.[6] The hydrolysis and alcoholysis of esters, often possessing coordinating cofunctionality, can be catalyzed by divalent metal ions such as Co^{2+}, Ni^{2+}, Zn^{2+}, and Cu^{2+} with k_{cat}/k_{uncat} values as large as 10^8.[7]

We have sought to develop a new method for catalyst selection based on the expected correlation between the binding affinity of transition state analogs (TSAs) to a catalyst center and the catalyst's activity and selectivity (Figure 1). A proof-of-concept demonstration of this principle was recently reported for the selection of hydrolytic catalysts by templating a set of imine-metal complexes, in equilibrium with their constituent aldehydes and amines, with TSAs.[8] A good correlation between ternary (imine)Zn(TSA) complex formation and the hydrolytic activity of the (imine)ZnX$_2$ complexes was found as predicted by the Pauling−Jenks model for enzyme and antibody catalysis.[9]

To apply this approach to high throughput combinatorial catalyst discovery, an efficient analytical method is needed to identify the binary and ternary metal-complexes present in large collections and to quantify the changes in composition resulting from challenging the system with potential substrates and TSAs. In our initial studies we employed reductive quenching of the imine-Zn complexes to the corresponding stable amine ligands that were analyzed and quantified by HPLC.[8] Although effective for small libraries, complete identification and quantification of large libraries of complexes would require extensive and customized separations for each library mixture and quantification would be laborious for lack of a universal detection method. ESI-MS has been found to be a good method for determining the composition and relative amounts of the species present in a solution under certain conditions.[17−21] This tool has been applied successfully to

Received: August 30, 2012
Revised: December 10, 2012
Published: December 16, 2012

   dx.doi.org/10.1021/co3001023 | ACS Comb. Sci. 2013, 15, 90−100

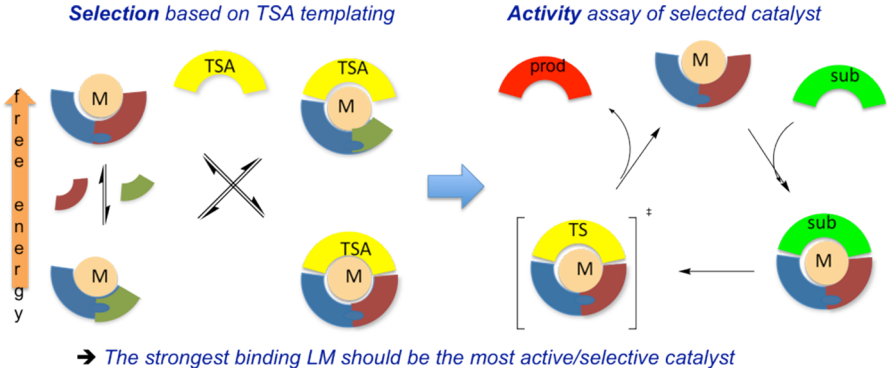

Figure 1. Relationship between binding of TSAs and catalytic activity/selectivity.

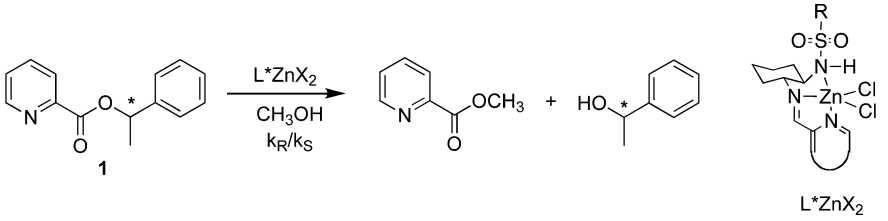

Figure 2. $LZnX_2$-catalyzed methanolysis of chiral picolinate ester.

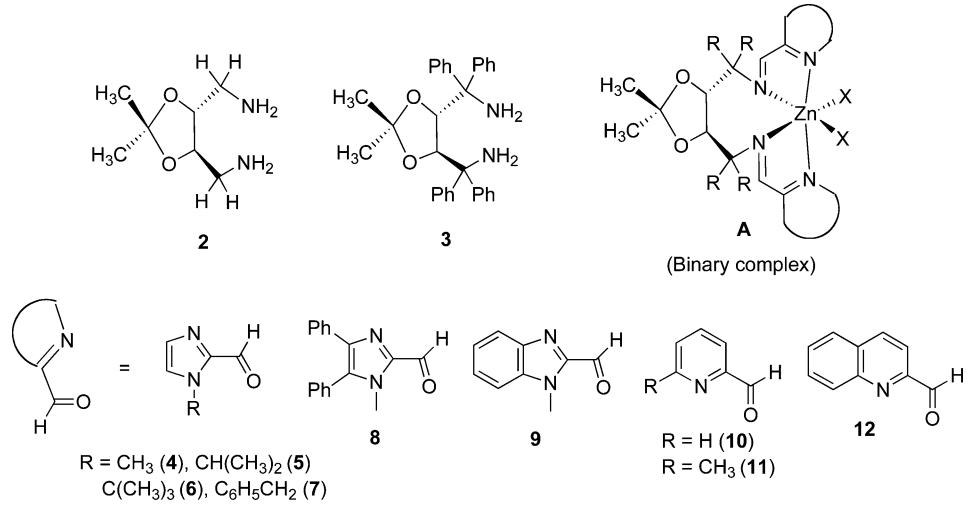

Figure 3. Building block amines and aldehydes for binary $LZn(OTf)_2$ complexes (**A**).

the characterization of various polynuclear metal complexes[22,23] and other noncovalent ligand-macromolecular associates, for example, ligand-DNA and ligand-protein complexes present in equilibrium.[12,24−26] In the present report we demonstrate the efficacy of ESI-MS as a tool for the identification and semiquantification of the composition of libraries of equilibrating $LZnX^+$, $LZnX(Sub)^+$, and $LZn(TSA)^+$ complexes.

Many valuable applications of catalysis derive from the catalyst's ability to control product selectivity. Stereoselective hydrolytic reactions, including kinetic resolutions, are particularly valuable synthetically.[10] Enzymatic enantioselective hydrolysis, alcoholysis, and transesterification reactions have achieved good efficiencies and are applied in the industrial production of optically active compounds, but their substrate scope is often limited. In contrast, the development of enantioselective solvolytic reactions using synthetic metal complex catalysts has been quite limited, the most notable success being achieved for the kinetic resolution of alkenyl esters, ethers, and azalactones,[11] of epoxides by $PdCl_2(MeCN)_2$ and $Cu(OAc)_2$-SEGPHOS,[12] and of amino acid esters by lanthanide-Schiff base complexes.[13] To date few systems have achieved good enantioselectivities, and the substrate scope has been quite limited. Hence, there is clearly a need for new classes of synthetic catalysts and reactions for kinetic resolution.

Seeking applications of the dynamic TSA-templating approach to catalyst selection we have targeted the kinetic resolution of chiral, racemic alcohols via their picolinate esters, employing homochiral imine-metal complex catalysts and suitable TSAs (Figure 2). The facile hydrolysis of coordinating picolinate esters has found use in organic synthesis, as a protecting group for alcohols (deprotected by MeOH/$Zn(OAc)_2$)[14] and in the Mitsunobu stereoinversion of alcohols (the picolinate removed by MeOH/$Cu(OAc)_2$).[15] In our initial investigation a series of bi/tridentate chiral Zn-(imine) complexes was prepared from mono-*N*-sulfonyl derivatives of (*1R,2R*)-diaminocyclohexane, *N*-heterocyclic aldehydes, and

dx.doi.org/10.1021/co3001023 | *ACS Comb. Sci.* 2013, 15, 90−100

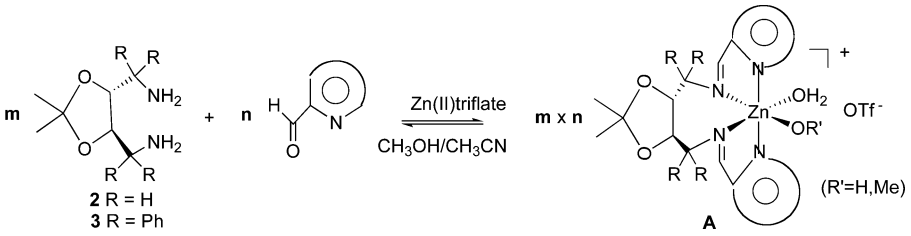

Figure 4. Generation of binary $LZn(OTf)^+$ (**A**) complexes.

zinc salts. The methanolysis rate of the chiral picolinate ester **1** catalyzed by these Zn-Schiff base complexes was found to vary approximately a hundred-fold and in a complex way depending on the imine ligand and the Zn-counteranion, k_{obs} = 5.0 × 10^{-6}–4.8 × 10^{-4} $M^{-1}sec^{-1}$.[16] However, selected L^*ZnX_2 complexes showed little difference (±10%) in their catalytic rates for hydrolysis of enantiomeric substrates, that is, enantioselectivities.

From our initial study we recognized the need both for an effective method to analyze the composition of larger libraries of metal complexes for high throughput screening and for improved chiral recognition/induction among the complexes. To improve enantioselectivity we sought tight-binding, higher denticity (4 vs 3) chiral polydentate ligands that would impose a more well-defined, chiral environment for the Zn-center in its coordination to chiral substrates and TSAs.

RESULTS AND DISCUSSION

In considering new ligand types we selected C2-chiral diamines **2** and **3** based on computational molecular models which indicated that the tetradentate Schiff base (diimine) complexes formed by condensation of these diamines with heterocyclic aldehydes would enforce a (nonplanar) tetrapodal geometry, leaving two *cis*-coordination sites to bind either a bidentate substrate or a monodentate substrate and an alkoxide or hydroxide nucleophile (Figure 3). Diamine ligands of this type were originally developed by Seebach et al.[27] Metal (Co, Cu, and Rh) complexes derived from these chiral diimines were recently prepared by Nindakova et al.,[28] and these complexes have seen a few applications in asymmetric metal-catalyzed reactions, including nitroaldol, transfer hydrogenation, and borohydride reduction of ketones[29] with variable enantioselectivities.[30]

1. Generation and Analysis of Binary $LZn(OTf)_2$ Complexes. The approach to and attainment of equilibrium at room temperature among sets (libraries) of the binary $LZn(OTf)_2$ complexes **A** could be monitored by ESI-MS. The complexes were generated in MeOH by combining one or more aldehyde(s) (each 2 equiv) with the diamine (1 equiv) and $ZnOTf_2$ (1 equiv) at room temperature (rt) (Figure 4). Sampling and analysis by ESI-MS over several hours revealed the formation of various $[LZn(OTf)]^+$ species as well as $[LZn(OCH_3)H_2O]^+$ and $[LZn(H_2O)OH]^+$ (Table 1; note H_2O is produced from aldehyde/amine condensation to the diimine L). Zinc-containing ions are easily recognized by their distinctive isotope pattern (^{64}Zn 48.6%, ^{66}Zn 27.9%, ^{68}Zn 18.8%). A constant composition and relative intensity (ion abundance) of ions compared to the added noninteracting salt, $Bu_4N^+PF_6^-$, was reached within 24 h, indicative of equilibrium being reached. It is noteworthy that Zn-containing species lacking coordinated L were not detected, indicating a large K_f for $LZnX^+$.[31] In library 1 all six possible binary complexes were detected, albeit with different ion counts. In library 2, however, only 6 of 14 possible binary complexes were detected with appreciable ion intensities, and in library 3 (derived from diamine **3**) only 9 of 21 possible complexes were detected. Although the ion abundances among the $[LZn(OTf)]^+$ complexes with different L may not be *quantitatively* correlated with their relative amounts because of their varying sizes, ligand variations and solvation, these observations indicate that the distribution of complexes in the libraries at equilibrium (and hence their relative stabilities) varies substantially. Both steric and electronic effects apparently influence the composition of the libraries as illustrated by the absence of complexes in libraries 2 and 3 derived from bulky aldehyde **6** and the differences in abundance among the complexes derived from the heterocyclic aldehydes of different basicities (imidazole, pyridine, quinoline). MS analysis of the binary (and subsequently ternary) complex libraries thus facilitates the

Table 1. Binary Complexes, $LZn(OTf)^+$ Detected by ESI-MS (CH_3OH)

library	binary complexes	*m/z* (found)[a]
Library 1[b]: diamine **2** + aldehydes **4,8,10** + $Zn(OTf)_2$	$[(\mathbf{2}–\mathbf{4}–\mathbf{10})^{64}Zn(OH)(H_2O)]^+$	440.1
	$[(\mathbf{2}–\mathbf{10}–\mathbf{10})^{64}Zn(OH)(H_2O)]^+$	437.1
	$[(\mathbf{2}–\mathbf{4}–\mathbf{4})^{64}Zn(OTf)]^+$	557.1
	$[(\mathbf{2}–\mathbf{8}–\mathbf{10})^{64}Zn(OH)(H_2O)]^+$	592.1
	$[(\mathbf{2}–\mathbf{4}–\mathbf{8})^{64}Zn(OH)(H_2O)]^+$	595.1
	$[(\mathbf{2}–\mathbf{8}–\mathbf{8})^{64}Zn(OH)(H_2O)]^+$	747.2
Library 2[b]: diamine 2 + aldehydes **5, 6, 7, 9, 11** + $Zn(OTf)_2$	$[(\mathbf{2}–\mathbf{5}–\mathbf{11})^{64}Zn(OCH_3)(H_2O)]^+$	498.2
	$[(\mathbf{2}–\mathbf{6}–\mathbf{11})^{64}Zn(OCH_3)(H_2O)]^+$	510.2
	$[(\mathbf{2}–\mathbf{5}–\mathbf{5})^{64}Zn(OCH_3)(H_2O)]^+$	513.2
	$[(\mathbf{2}–\mathbf{9}–\mathbf{11})^{64}Zn(OCH_3)(H_2O)]^+$	518.2
	$[(\mathbf{2}–\mathbf{9}–\mathbf{9})^{64}Zn(OCH_3)(H_2O)]^+$	557.2
	$[(\mathbf{2}–\mathbf{7}–\mathbf{7})^{64}Zn(OCH_3)(H_2O)]^+$	609.2
Library 3[c]: diamine **3** + aldehydes **4, 5, 6, 7, 8, 9** + $Zn(OTf)_2$	$[(\mathbf{3}–\mathbf{4}–\mathbf{5})^{64}Zn(OTf)]^+$	889.2
	$[(\mathbf{3}–\mathbf{4}–\mathbf{9})^{64}Zn(OTf)]^+$	911.2
	$[(\mathbf{3}–\mathbf{5}–\mathbf{5})^{64}Zn(OTf)]^+$	917.2
	$[(\mathbf{3}–\mathbf{5}–\mathbf{9})^{64}Zn(OTf)]^+$	939.2
	$[(\mathbf{3}–\mathbf{9}–\mathbf{9})^{64}Zn(OTf)]^+$	961.2
	$[(\mathbf{3}–\mathbf{7}–\mathbf{9})^{64}Zn(OTf)]^+$	987.3
	$[(\mathbf{3}–\mathbf{7}–\mathbf{7})^{64}Zn(OTf)]^+$	1013.2
	$[(\mathbf{3}–\mathbf{5}–\mathbf{8})^{64}Zn(OTf)]^+$	1041.3
	$[(\mathbf{3}–\mathbf{8}–\mathbf{9})^{64}Zn(OTf)]^+$	1063.3
	$[(\mathbf{3}–\mathbf{7}–\mathbf{8})^{64}Zn(OTf)]^+$	1089.2

[a] *m/z* corresponding to ^{64}Zn (48.6% isotopic abundance). [b] Library 1 and 2 is produced in MeOH. [c] Library 3 is produced in CH_3CN.

dx.doi.org/10.1021/co3001023 | *ACS Comb. Sci.* 2013, 15, 90–100

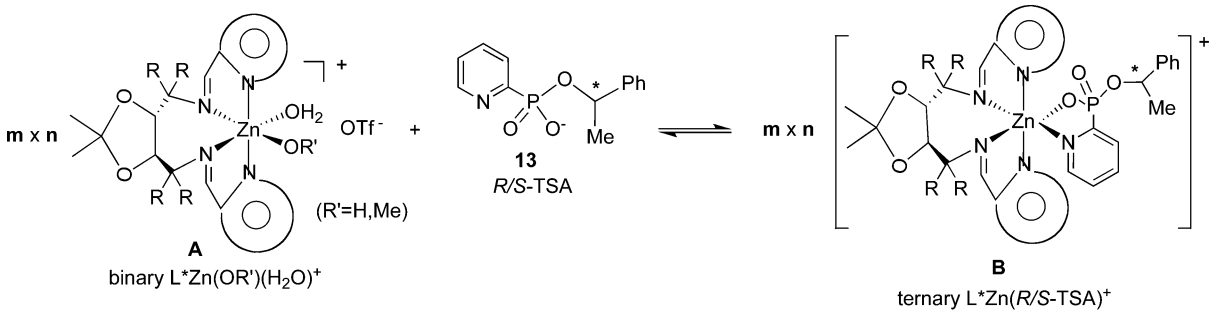

Figure 5. Formation of ternary LZn(TSA)$^+$ complexes.

identification of the most energetically favored species and the selection of promising candidates for synthesis and individual catalytic screening, minimizing time spent on less promising candidates.

2. Generation and Analysis of Ternary LZn(TSA)$^+$ Complexes. Phosphonate esters have been employed as carboxyl ester hydrolytic TSAs, mimicking the putative hydrolytic pseudotetrahedral transition state geometry.[32] For the Pyr-CO_2R substrates of this study corresponding phosphonate derivatives, *R*- and *S*-Pyr-PO(OH)CHMePh (**13**) were selected and prepared from their respective enantiomeric benzylic alcohols (Figure 5).[33] These compounds were expected to bind to the (diimine)Zn^{n+} species in an *N,O*-bidentate mode mimicking the transition state and intermediate from hydroxide/alkoxide attack on the Zn-activated pyridine ester.[7a,33,34]

Binding of the (diimine)Zn(OTf)$^+$ to the pyridyl phosphonate TSA **13** and the composition of the resulting ternary LZn(**13**)$^+$ complexes was established by the Job plot (continuous variation) method[8,16] and by ESI-MS. Thus, ^{1}H NMR monitoring of the chemical shift (δ) of the imine proton signal (C<u>H</u>═N-) of the LZn-species derived from diamine **2** and imidazole aldehyde **6** as a function of the LZn/TSA(**13**) ratio provided a plot with a single maximum at LZn/**13** = 1 (Figure 6), supporting the formation of a ternary complex of composition [LZn(**13**)]$^+$.

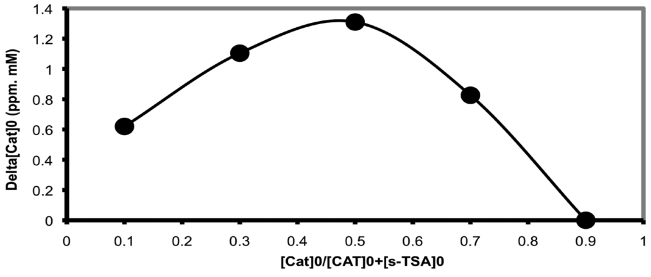

Figure 6. Job plot for the complexation (**2**−**6**−**6**)Zn(OTf)$^+$ with *S*-TSA (**13**) at a total concentration of 10 mM in CD_3OD; weighted value of imine proton NMR chemical shift $\delta \times$ complex concentration [mM] (*x*-axis) as a function of [cat]^0/[cat]^0+[*S*-TSA]^0 (*y*-axis).

ESI-MS analysis of solutions of both individual and sets of (diimine)Zn(OTf)$_2$ complexes after treatment with *R*- or *S*-TSA **13** also showed the formation of ternary LZn(TSA-**13**)$^+$ complexes. Treatment of binary complex library 1, derived from diamine **2**, aldehydes (**4**,**8**,**10**), Zn(OTf)$_2$ with TSA-**13** under equilibrating conditions showed the formation of three (out of 6 possible) LZn(**13**)$^+$ ternary complexes for each enantiomer of **13**: [(**2**−**4**−**10**)Zn(**13**)]$^+$, [(**2**−**8**−**10**)Zn(**13**)]$^+$, and [(**2**−**8**−**8**)Zn(**13**)]$^+$ (library 4, Table 2). A constant composition and relative intensity of ions is reached within approximately five minutes when normalized to the concentration of non-coordinating salt $Bu_4N^+PF_6^-$ added as an internal reference (Figure 7).

Table 2. ESI-MS of Ternary Complexes [LZn(*R*/*S*-TSA (13)]$^+$[a]

library	ternary complexes	*m*/*z* (found)
Library 4: diamine **2** + aldehyde **4**,**8**,**10** + Zn(OTf)$_2$ + *R*- or *S*-**13**	[(**2**−**4**−**10**)^{64}Zn(**13**)]$^+$	667.2
	[(**2**−**8**−**10**)^{64}Zn(**13**)]$^+$	819.2
	[(**2**−**8**−**8**)^{64}Zn(**13**)]$^+$	917.3
Library 5: diamine **2** + aldehyde **5**,**6**,**7**,**9**,**11** + Zn(OTf)$_2$ + *R*- or *S*-**13**	[(**2**−**5**−**5**)^{64}Zn(**13**)]$^+$	726.3
	[(**2**−**5**−**6**)^{64}Zn(**13**)]$^+$	740.3
	[(**2**−**5**−**9**)^{64}Zn(**13**)]$^+$	748.2
	[(**2**−**6**−**6**)^{64}Zn(**13**)]$^+$	754.3
	[(**2**−**6**−**9**)^{64}Zn(**13**)]$^+$	762.3
	[(**2**−**5**−**7**)^{64}Zn(**13**)]$^+$	774.3
	[(**2**−**6**−**7**)^{64}Zn(**13**)]$^+$	788.3
	[(**2**−**7**−**9**)^{64}Zn(**13**)]$^+$	796.2
	[(**2**−**7**−**7**)^{64}Zn(**13**)]$^+$	822.3

[a]Amine **2** (0.05 mM), aldehyde (0.10 mM), zinc triflate (0.05 mM), and Bu_4NPF_6 (0.05 mM, internal standard) are mixed in methanol overnight (rt).

Similarly, treatment of library 2 (from **2**, aldehydes- **5**, **6**, **7**, **9**, **11** + Zn(OTf)$_2$) with *R*- or *S*-**13** revealed the formation of ternary complexes LZn(**13**)$^+$ by ESI-MS (library 5, Table 2). Among 15 possibilities, we detected a common set of 9 LZn(TSA-**13**)$^+$ complexes with either enantiomer of **13**. A summary of the ternary complexes detected is given in Table 2.

Although the ion abundances among LZn(TSA)$^+$ with different auxiliary Ls may not be quantitatively correlated with concentration, one can expect that the ion detection response for pairs of *diastereomeric* LZn(TSA)$^+$ complexes *that have the same ligand L* and *enantiomeric* TSAs should be very similar.[35] Hence, with the inclusion of an inert reference compound, parallel reactions of the LZn(OTf)$_2$ libraries with the *R*- and *S*-TSAs **13** with ESI-MS-analysis were conducted to

dx.doi.org/10.1021/co3001023 | ACS Comb. Sci. 2013, 15, 90−100

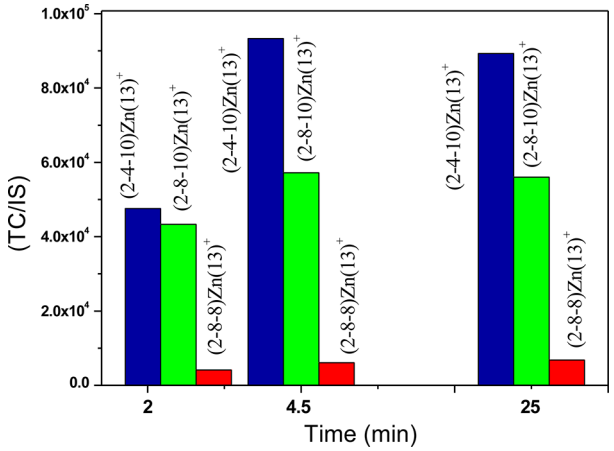

Figure 7. Time-dependent ESI−MS monitoring of ternary complexes from library 1 + *R*-TSA (**13**) = library 4; TC = ion count of complex, IS = ion count of internal standard, Bu_4N^+ PF_6^-.

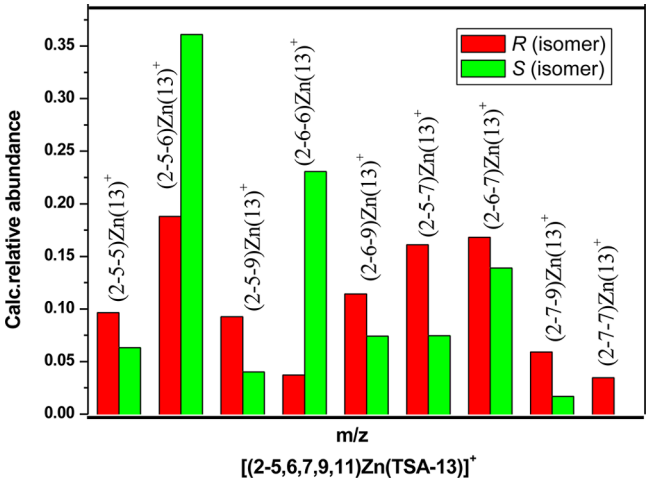

Figure 9. Amplification of LZn(**13**)$^+$ from (**2**-**5**, -**6**, -**7**, -**9**, -**11**)Zn$(OTf)_2$ + *R*- *or* *S*-**13** analyzed by ESI-MS at 24 h. The calculated relative abundance = (ion count of peak/ion count of internal standard)/sum over all ions of (ion count of peak/ion count of internal standard).

determine the relative binding affinities, that is, the stereodiscrimination (selectivity) factor, α, of the various LZn$(OTf)^+$ complexes toward the enantiomeric TSAs. Figure 8 shows a section of the ESI-mass spectra for the ternary complexes produced from the enantiomeric TSAs **13** and the LZn complexes of library 2 = library 4. An amplification graph (Figure 9) is produced by plotting the (**2**-**n**-**n**)Zn(*R*- or *S*-**13**) signal intensity divided by the intensity of the $Bu_4N^+PF_6^-$ internal standard (% TC/IS; TC = total ion current; IS = ion current of internal standard) versus m/z of LZn(**13**)$^+$. From this graph one can see small *R*-binding preferences ($\leq$2:1) are found for L = **2**−**5**−**5**, **2**−**5**−**9**, **2**−**6**−**9**, and **2**−**6**−**7**; a larger (>2:1) *R*-selectivity is seen with **2**−**5**−**7** and **2**−**7**−**9**. Binding of the *S*-TSA is preferred moderately (ca. 2:1) for complex with L = **2**−**5**−**6**, and the most *S*-selective complex (ca. 5:1) was found for L = **2**−**6**−**6**. This latter selectivity corresponds to approximately a 1.0 kcal difference at equilibrium in favor of the (**2**−**6**−**6**)Zn(*S*-**13**)$^+$ complex. We could not detect ternary complex formation in library mixtures derived from the tetraphenyldiamine **3** with TSA **13** by ESI-MS because of the formation of precipitates that were poorly soluble in all solvents tested. We suspect that these intractable materials are either $Zn(TSA)_2$[36] or possibly polynuclear $[Zn(L)(TSA)]_n$ which could result from weaker binding of the sterically hindered ligands derived from **3**. The convenient and rapid ESI-MS analysis of the combinatorial libraries of binary LZn(OTf)-complexes from diamine **2** with the enantiomeric TSAs, *R*- and *S*-**13**, facilitates the identification and selection of candidate catalysts for testing, avoiding the more labor intensive, one-at-a-time preparation and separate testing of all possible candidates.

3. Formation of LZn(Sub)$^+$. The rate acceleration induced by a catalyst is considered to be the result of differential binding stabilization of the substrate relative to the transition state, as reflected in the activation energy. It was of interest, therefore, to assess the binding affinity and here, especially the enantiodifferentiation of the chiral substrate, *S*-ester, by the chiral LZn complexes (Figure 10). Complexation of ester *S*-**1** by the polyimine complexes Zn(**2**−**6**−**6**)$(OTf)_2$ and Zn(**2**−**9**−**9**)-$(OTf)_2$ was suggested by NMR spectroscopy, which shows a continuous shifting of the imine N−H signal as a function of the added substrate **1** (in acetonitrile). The resulting Job plot (see Supporting Information) showed maxima at both 1:1 and approximately 9:1 Sub/Zn ratios, suggesting the formation of ternary complexes LZn$(\mathbf{1})_1^{2+}$ and, probably, LZn$(\mathbf{1})_2^{2+}$. Parallel ESI-MS experiments with Zn(**2**−**6**−**6**)$(OTf)_2$ and *R*- or *S*-ester

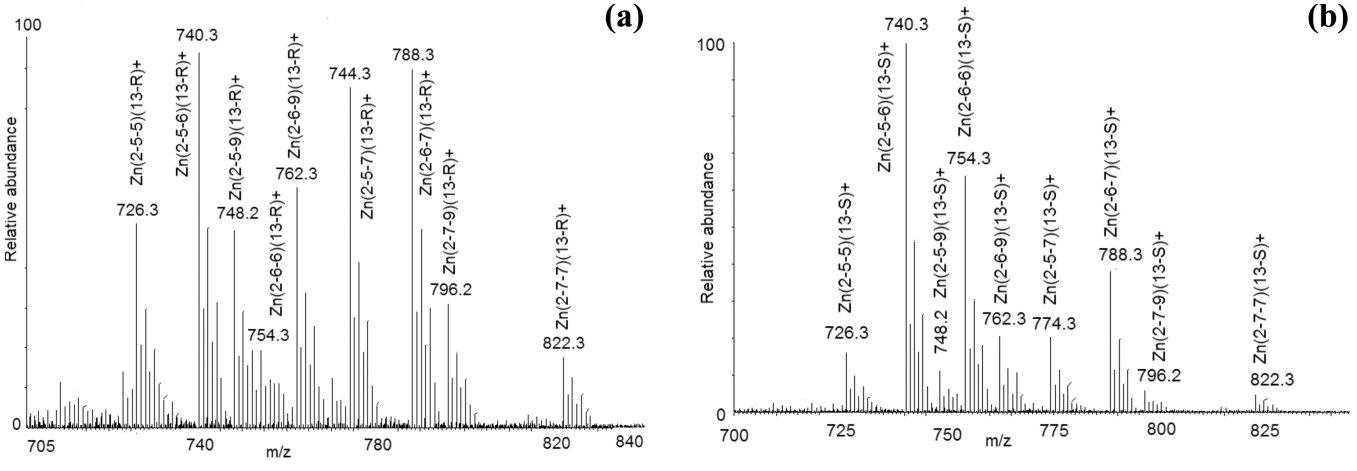

Figure 8. Portion of ESI-MS of (a) (**2**-**5**, -**6**, -**7**, -**9**, -**11**)Zn$(OTf)_2$ + *R*-**13**; and (b) (**2**-**5**, -**6**, -**7**, -**9**, -**11**)Zn$(OTf)_2$ + *S*-**13**; at 24 h in MeOH.

dx.doi.org/10.1021/co3001023 | *ACS Comb. Sci.* 2013, 15, 90−100

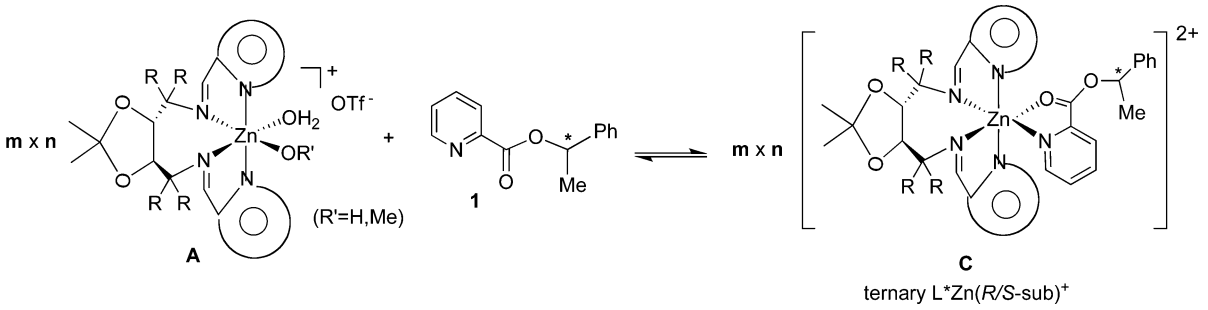

Figure 10. Formation of ternary LZn(substrate)$^+$ complexes.

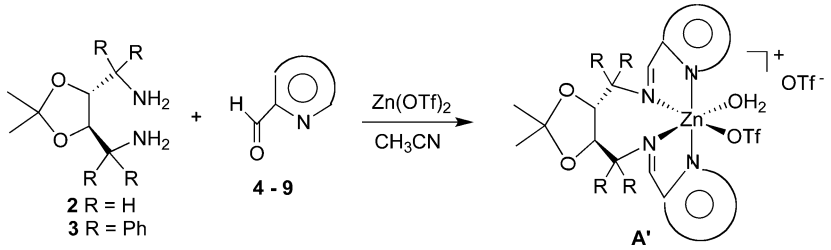

Figure 11. Preparation of isolable binary LZn(OTf)$^+$ complexes.

1 in acetonitrile (1:1) also revealed the formation of (**2**−**6**−**6**)-Zn(**1**)$^{2+}$ (m/z = 360) upon addition of 1 equiv of **1** (Figure 10). Comparison of the ion intensities of the diastereomeric ternary complexes relative to the internal standard indicated almost equal concentrations, ± 10%, and thus little stereodifferentiation of the enantiomeric substrate esters by (**2**−**6**−**6**)Zn(OTf)$_2$, which contrasts with that observed with the corresponding complexes of the TSA **13** (Figure 7). This indicates a greater chiral discrimination of the phosphonate TSA relative to the substrate ester for these chiral Zn-complexes and supports the idea that the primary determinants of enantioselectivity are steric and electronic interactions in the reaction's transition state.

4. Isolation-Characterization of Binary LZn(OTf)$_2$ Complexes. To authenticate the LZn-complexes revealed by ESI-MS in the combinatorial libraries 1−3 and to provide samples for catalytic testing, we prepared and characterized several complexes with symmetrical diimine ligands (i.e., derived from two identical aldehydes). These were prepared by combining either of the chiral diamines **2** or **3** with the *N*-heterocyclic aldehydes (**4**−**12**) and Zn(OTf)$_2$ in acetonitrile at reflux (Figure 11). Their ^{1}H NMR spectra exhibited characteristic imine N=C<u>H</u> resonances at δ 8.2−9.2 ppm. ESI-mass spectra (CH_3CN) indicated the presence of [LZn(OTf)]$^+$OTf$^-$ and [LZn(OTf)(H_2O)]$^+$OTf$^-$ as major species with the characteristic isotope pattern for Zn-containing ions (^{64}Zn 48.6%, ^{66}Zn 27.9%, ^{68}Zn 18.8%). Elemental composition was confirmed by high resolution ESI-MS showing the coordination of LZn(OH)/MeOH and H_2O (Table 1). The IR spectra of LZn(OTf)$_2$ displayed a sharp peak at 1600−1660 cm^{-1} for coordinated C=N and an absorption at 1200−1260 cm^{-1} for OTf$^-$.[37] Complexes incorporating the tetraphenyl-amine **3** and various aldehydes were generated similarly, but not isolated, and were also identified by ESI-MS.

5. Kinetic Studies of Esterolysis Catalyzed by LZn-(OTf)$_2$. The following LZn(OTf)$_2$ were selected and evaluated for catalytic activity, L= [**2**−**4**−**4**]-, [**2**−**5**−**5**]-, [**2**−**6**−**6**]-, [**2**−**9**−**9**]-, [**3**−**5**−**5**]-, [**3**−**6**−**6**]-, [**3**−**8**−**8**]-, [**3**−**9**−**9**]. Most of these candidates were initially detected by MS in the binary complex libraries 1−3 and similarly found to form ternary LZn(TSA-**13**)$^+$ complexes in libraries 4,5. The catalytic activity and enantioselectivity of the LZn(OTf)$_2$ complexes **A** were assessed by determining the initial rates (up to 15% conversion) of methanolysis of the *R*- and *S*- 1-phenylethyl picolinate (PEP, **1**) in the presence of 0.1−1.0 mol % catalyst at T = 292 K by ^{1}H NMR monitoring (Figure 12). The decline of

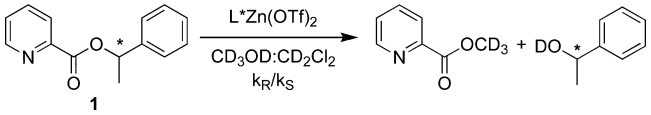

Figure 12. LZn(OTf)$_2$-catalyzed methanolysis of ester **1**.

the ester methyl doublet and a corresponding growth of the product alcohol methyl doublet (Figure 13) were integrated to provide concentration vs time plots that lead to the initial rates (Figure 14) and second order rate constants listed in Table 3. Three independent methanolysis runs on **1** catalyzed by [**2**−**5**−**5**]Zn(OTf)$_2$ showed good agreement (±5%) among their rate constants, 2.0 × 10^{-6} M^{-1}s^{-1}.

The solvolytic rate constants depend markedly on the catalyst structure (Figure 3, Table 3). The catalytic activities of the imidazole-based complexes [**2**−**4**−**4**]-, [**2**−**5**−**5**]-, and [**2**−**6**−**6**]-Zn(OTf)$_2$ are similar, whereas the activity of benzimidazole derivative [**2**−**9**−**6**]Zn(OTf)$_2$ is considerably greater. Complexes derived from the tetraphenyl-diamine **3**, [**3**−**5**−**5**]-, [**3**−**6**−**6**]-, and [**3**−**12**−**12**]Zn(OTf)$_2$, are 1−2 orders of magnitude more active than those from diamine **2**; but the benzimidazole derivative [**3**−**9**−**9**]Zn(OTf)$_2$ is less active, comparable to [**2**−**4**−**4**]-, [**2**−**5**−**5**]-, and [**2**-**6**−**6**]-Zn(OTf)$_2$. The greater activity of benzimidazole-based complexes may be the result of the lower basicity of the ligand (i.e., pK_a 6.9 vs pK_a 5.4),[38] providing a more electrophilic LZn(sub)$^+$ complex, which enhances the susceptibility of the ester C=O to nucleophilic attack by MeOH. The greater activity of the tetraphenyl derivatives is more surprising, since the electronic differences between the parent H_4- and the Ph_4-ligands are

dx.doi.org/10.1021/co3001023 | ACS Comb. Sci. 2013, 15, 90−100

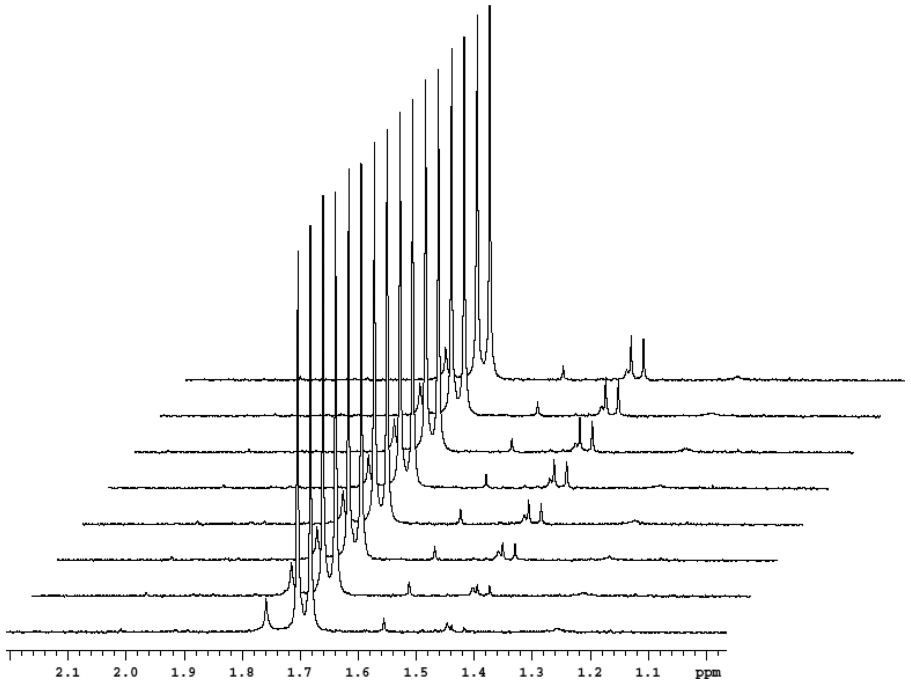

Figure 13. Time-dependent ^{1}H NMR spectra of *R*-**1** ester reaction in CD_3OD/CD_2Cl_2 (1:1) catalyzed by 1 mol % of [**2**−**6**−**6**]Zn(OTf)$_2$; spectra, recorded at 2 min intervals.

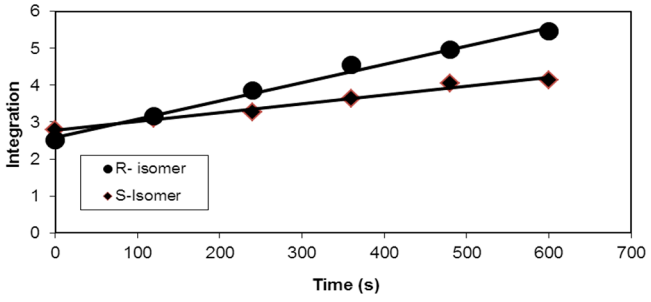

Figure 14. Time-dependent PhCH(OD)Me formation in reaction of *R- and S*-**1** in CD_3OD/CD_2Cl_2 (1:1) with 1 mol % [**2**−**6**−**6**]Zn(OTf)$_2$.

Table 3. Rate Constants for Methanolysis of *R*- and *S*-1 Catalyzed by L*Zn(OTf)$_2$[a,b]

entry	catalyst (loading)	k_R (M^{-1} s^{-1})	k_S (M^{-1} s^{-1})	k_R/k_S
1	[**2**−**4**−**4**]Zn(OTf)$_2$ (1 mol %)	2.3×10^{-6}	2.3×10^{-6}	1.0
2	[**2**−**5**−**5**]Zn(OTf)$_2$ (1 mol %)	2.0×10^{-6}	2.0×10^{-6}	1.0
3	[**2**−**6**−**6**]Zn(OTf)$_2$ (1 mol %)	5.0×10^{-6}	2.4×10^{-6}	2.1
4	[**2**−**9**−**9**]Zn(OTf)$_2$ (1 mol %)	2.6×10^{-5}	2.8×10^{-5}	0.93
5	[**3**−**5**−**5**]ZnOTf$_2$ (0.1 mol %)	8.3×10^{-5}	3.5×10^{-5}	2.3
6	[**3**−**6**−**6**]Zn(OTf)$_2$ (0.1 mol %)	1.1×10^{-4}	3.7×10^{-5}	2.8
7	[**3**−**8**−**8**]Zn(OTf)$_2$ (0.5 mol %)	7.9×10^{-5}	5.4×10^{-5}	1.4
8	[**3**−**9**−**9**]Zn(OTf)$_2$ (0.5 mol %)	4.4×10^{-6}	5.8×10^{-6}	0.76
9	[**3**−**12**−**12**]Zn(OTf)$_2$ (1 mol %)	2.5×10^{-5}	1.6×10^{-5}	1.5

[a][*R*- and *S*-**13**]$_0$ = 10 mM, [catalyst] = 0.10 mM, 0.050 mM, and 0.010 mM in 1:1 CD_3OD/CD_2Cl_2 (T = 292 K). [b]Selected runs repeated in triplicate gave rate constants with values within ±5%.

likely to be small. We speculate that the increased steric demand of the latter ligand could accelerate a dissociative step in the solvolytic mechanism, for example, facilitating chelate arm decoordination to alleviate strain and enabling MeOH coordination/activation with an enhanced reaction rate. We observed significantly greater selectivity with some of the present tetradentate-Zn catalysts compared to our previous tridentate LZn-complexes.[15] Regardless of cause, the (**3**-**x**-**y**)Zn(OTf)$_2$ complexes are among the more active esterolytic Zn-catalysts reported to date.[7,15,16]

Key features of the kinetic enantioselectivity factors, k_R/k_S = α, displayed by the various catalysts include (Table 3) the following: (1) the values range from nil to moderate, with the better selectivities coming from [**2**−**6**−**6**]-, [**3**−**5**−**5**]-, and [**3**−**6**−**6**]Zn(OTf)$_2$ catalyzing the faster methanolysis of the *R*-ester; and (2) the benzimidazole-derived catalysts [**2**−**9**−**9**]Zn(OTf)$_2$ and [**3**−**9**−**9**]Zn(OTf)$_2$ exhibit a small kinetic selectivity for the *S*-ester solvolysis. There appears to be a modest correlation between the stereoselectivity and steric demands of the ligand, for example, the *t*-Bu-imidazole-derived complex [**2**−**6**−**6**]Zn(OTf)$_2$ is more selective than the -NMe, and -NPr^i derivatives, and the tetraphenyl-derived complexes (entries 5−9) generally show greater enantioselectivity than those derived from the diamine **2** (entries 1−4). Disappointingly, none of these catalysts exhibit the level of enantioselectivity that would enable an effective kinetic resolution, for example, $\alpha \geq 10$.[6,10,39] However, the better selectivities displayed by the present chiral complexes are comparable to those reported previously for synthetic metal complex-based esterolytic catalysts. What then may be the reason for the modest chiral discrimination displayed by the present LZn complexes? The possibility that this is the result of competing catalysis by an achiral Zn-species such as Zn(solvent)(OTf)$_2$ was evaluated (as per a reviewer's suggestion). Indeed, it was found that methanolysis of ester **1** is catalyzed by Zn(OTf)$_2$ (in the absence of a tetramine L) with a rate constant, k = 6.8 ×

dx.doi.org/10.1021/co3001023 | *ACS Comb. Sci.* 2013, 15, 90−100

10^{-5} M^{-1} s^{-1}, comparable to the complexes derived from **3** and about 10-fold greater than by those derived from **2** (Table 3). Nonetheless, the absence of MS-detectable free Zn species in solutions of ligands **2** and **3** + $Zn(OTf)_2$ (op cit) and the proven high affinity binding of tetradentate amines for Zn(ii) ($K_f = 10^8-10^{11}$)[31] provide evidence that unselective catalysis of ester solvolysis by (solvated) zinc ion is unlikely to make a significant contribution to the reaction rates and selectivity. A more likely factor is imperfect transfer of chirality from the L-Zn complexes to the bound transition state. Supporting this notion, preliminary PM3 and DFT molecular modeling calculations of selected diastereomeric ternary L*Zn-complexes of *R*- and *S*-**13** show small energy differences of 0−3 kcal.

One of the goals of this study was to assess the correlation between the enantioselectivity of substrate and TSA-binding to the $L^*Zn(OTf)_2$ complexes and their catalytic enantioselectivity. No appreciable substrate (**1**) binding selectivity was detected with [**2**−**6**−**6**]$Zn(OTf)_2$ which exhibits appreciable kinetic selectivity. This supports the idea that stereoinduction in the solvolytic reactions catalyzed by $(L^*)Zn(OTf)_2$ is achieved in the tetrahedral transition state or intermediate rather than from stereoselective substrate binding. This feature contrasts with a report of MS-based selection Pd-catalysts for allylic substitution in which intermediate stability correlated inversely with regioselectivity.[40] For a variety of reasons we were only able to obtain both TSA-binding and kinetic selectivity results with two complexes, [**2**−**5**−**5**]$Zn(OTf)_2$ and [**2**−**6**−**6**]$Zn(OTf)_2$. Although the latter does exhibit both greater binding and kinetic selectivity than the former, the configurational preferences of [**2**−**6**−**6**]$Zn(OTf)_2$, *S* for binding and *R* for reactivity, are opposite. Several explanations for this disparity can be envisioned. One that we favor is that the $LZn(TSA)^+$ does not provide an accurate representation of the electronic and geometrical characteristics of the reaction's stereodefining step. We note that pyridine-$PO_2(OR^*)^-$ is best suited as a hydrolytic TSA (OH as attacking Nu) and does not include a methoxy group on the *P*-atom that would mimic that of the approaching MeOH involved in forming the tetrahedral intermediate (**B**, Figure 15). Efforts are underway to prepare and test the binding affinity and stereoselectivity of such a phosphodiester (**D**).

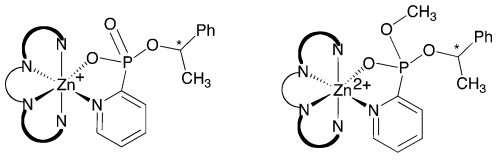

B **D**

Figure 15. Tetradentate zinc complexes with TSA **13** (**B**) and a phosphodiester (**D**).

CONCLUSIONS

Individual and dynamic libraries of chiral tetradentate N_4-diimine-$Zn(OTf)^+$ complexes have been prepared from tartrate-derived diamines and various *N*-heterocyclic aldehydes. ESI-MS analysis allows convenient determination of the composition of the species in the library at equilibrium and the change in library composition upon the addition of a coordinating chiral substrate and enantiomeric phosphonate TSAs. Binding studies of the $(diimine)Zn(OTf)_2$ complex libraries by ESI-MS analysis with enantiomeric *R*- and *S*-2-pyridyl phosphonate TSA **13** show chiral discrimination via formation of diastereomeric $LZn(R/S\text{-}\mathbf{13})^+$ complexes with low to moderate enantioselectivity ratios, k_R/k_S (α), ranging from 0.5 to 5.0, whereas templating with the enantiomeric substrates, $PyrCO_2CH(OH)Ph$ (**1**), show negligible chiral recognition. The rate constants for methanolysis of the *R*- and *S*-esters, $PyrCO_2CH(OH)Ph$, catalyzed by several BIN complexes vary several fold over the set of L* and with enantioselectivity factors ranging from 1.0 to 2.5. This dynamic combinatorial approach to the generation and MS-screening of metal complex libraries provides a new and convenient methodology for high throughput catalyst discovery. Its capability for templating with substrates, TSAs or product analogs can be the basis for selection of metal complex catalysts with high activity or selectivity.

EXPERIMENTAL PROCEDURES

Materials and General Methods. Commercially available reagents were used as received. *R*- and *S*-1-Phenylethanol picolinic acid ester (**1**) and *R*- and *S*-1-phenylethanol pyridine-2-phosphonic acid ester (**13**) were prepared by literature procedures.[41] (4*R*,5*R*)-2,2-Dimethyl-1,3-dioxolane-4,5-dimethanamine (**2**) and (4*R*,5*R*)-bis-(aminodiphenylmethyl)-2,2-dimethyl-1,3-dioxolane (**3**) were prepared and purified by a literature procedure.[30,42] The aldehyde precursors *N*-isopropyl-imidazole, *N*-*tert*-butyl-imidazole, *N*-benzylimidazole, 4,5-diphenylimidazole, and *N*-methyl-4,5-diphenylimidazole were prepared by reported procedures.[43,44] The heterocyclic aldehydes **5**−**9** were prepared by a modification of the procedure reported by Katritsky[45] (see Supporting Information).

Infrared spectra (4000−500 cm^{-1}) were recorded as KBr pellets. ^1H- (300 MHz), ^{13}C- (60 MHz) NMR spectra were obtained and referenced to TMS as internal standard on a Varian Mercury 300 spectrometer. The molecular mass of the compounds was determined (methanol or acetonitrile solution) by the observed formula *m*/*z* peak. Low resolution MS data were obtained on a Micromass/Waters QTOF-1 equipped with an electrospray ionization source in the positive ion mode. Nitrogen gas was used as a nebulizing and drying gas with capillary voltage 3.0 kV, cone voltage ramp 10−85 V, source block temperature 120 °C, desolvation temperature 150 °C, and desolvation flow rate 200 L/h. High resolution MS Data were collected and analyzed on an Agilent 6538 UHD Accurate Mass QTOF equipped with an electrospray ionization source in positive ion mode. Nitrogen gas was used as a nebulizing and drying gas with the drying gas temperature of 325 °C and 10 L/min flow rate; the fragmentor voltage was 160 V and capillary voltage 3500 V.

Preparation of $LZn(OTf)_2$ Complexes. The synthesis of [Zn(**2**−**4**−**4**)$(OTf)_2$] (below) is typical of that used for all the complexes. The diamine **2** (0.50 mmol) was dissolved in 25 mL of dry acetonitrile. To this solution an acetonitrile solution of *N*-methylimidazole carboxaldehyde (1.0 mmol in 25 mL) was added, followed by zinc triflate (0.50 mmol) dissolved in 10 mL of acetonitrile. The resulting mixture was refluxed overnight, then the solvent was evaporated and the residual solid was triturated with small portions of diethyl ether to obtain the spectroscopically pure product.

[Zn(2−4−4)(OTf)$_2$]. ESI-HRMS (CH_3CN) found: *m*/*z* = 557.0761, calcd for $C_{18}H_{24}N_6O_5S^{64}ZnF_3^+$ = 557.0772; IR (KBr): 3392, 2991, 1635, 1500, 1425, 1259, 1163, 632; ^1H NMR (CD_3CN, δ_{ppm}): 8.68 (s, 2H), 7.48 (d, 2H, *J* = 1.2 Hz), 7.19 (s, 2H), 4.15 (d, 2H, *J* = 11.1 Hz), 4.06 (d, 2H, *J* = 4.8 Hz), 4.0 (m, 2H), 2.84 (s, 4H), 1.44 (s, 6H).

[Zn(2−5−5)(OTf)$_2$]. ESI-HRMS (CH_3CN) found: *m*/*z* = 613.1396, calcd for $C_{22}H_{32}N_6O_5S^{64}ZnF_3^+$ = 613.1398; IR (KBr): 3400, 2989, 1631, 1485, 1269, 1163, 1028, 638; ^1H NMR (CD_3CN, δ_{ppm}): 8.72 (s, 2H), 7.64 (d, 2H, *J* = 1.8 Hz), 7.28 (s, 2H) 4.89 (m, 2H), 4.17 (d, 2H, *J* = 9.9 Hz), 4.06 (d, 2H, *J* = 1.8 Hz), 4.0 (m, 2H), 1.57, 1.55 (dd, 12H, *J* = 1.2 Hz, 1.8 Hz), 1.45 (s, 6H).

[Zn(2−6−6)(OTf)$_2$]. ESI-HRMS (CH_3CN) found: *m*/*z* = 641.1717, calcd for $C_{24}H_{36}N_6O_5S^{64}ZnF_3^+$ = 641.1711; IR (KBr): 3133, 2992,

dx.doi.org/10.1021/co3001023 | ACS Comb. Sci. 2013, 15, 90−100

1630, 1520, 1437, 1240, 572; ^{1}H NMR (CD_3OD, δ_{ppm}): 9.20 (s, 2H), 7.85 (d, J = 8.5 Hz, 2H), 7.35 (d, J = 8.7 Hz, 2H), 4.42 (d, 2H, J = 12.6 Hz), 4.13 (m, 4H), 1.84 (s, 18H), 1.64 (s, 6H).

[Zn(2−9−9)(OTf)$_2$]. ESI-HRMS (CH_3CN) found: m/z = 657.1081, calcd for $C_{26}H_{26}N_6O_5S^{64}ZnF_3^+$ = 657.1085; IR (KBr): 3393, 2988, 1638, 1495, 1272, 1033, 926, 746, 642, 573, 516; ^{1}H NMR (CD_3CN, δ_{ppm}): 9.0 (s, 2H), 7.85 (d, 2H, J = 8.7 Hz), 7.60 (d, 2H, J = 8.4 Hz), 7.43 (m, 4H), 4.28 (d, 4H, J = 9.9 Hz), 4.10 (s, 6H), 4.0 (m, 2H), 1.46 (s, 6H).

[Zn(3−5−5)(OTf)$_2$]. ESI-HRMS (CH_3CN) found: m/z = 917.2648, calcd for $C_{46}H_{48}N_6O_5S^{64}ZnF_3^+$ = 917.265; IR (KBr): 3324, 1612, 1497, 1237, 1071, 1004, 888, 751, 710, 625, 574, 515; ^{1}H NMR (CD_3CN, δ): 8.23 (s, 2H), 7.68−7.0 (m, 14H), 4.19 (s, 2H), 1.56 (d, J = 6.6 Hz, 12H), 1.10 (s, 6H).

[Zn(3−6−6)(OTf)$_2$]. ESI-HRMS (CH_3CN) found: m/z = 945.2948, calcd for $C_{48}H_{52}N_6O_5S^{64}ZnF_3^+$ = 945.2963; IR (KBr): 3147, 2985, 1658, 1606, 1469, 1379, 1244, 1159, 1095, 1028, 877, 758, 702, 636, 514 cm^{-1}; ^{1}H NMR (CD_3CN, δ): 8.2 (s, 2H), 7.51−7.24 (m, 20H), 4.20 (s, 2H), 1.18 (s, 3H), 1.58 (s, 18H), 1.56 (s, 3H).

[Zn(3−8−8)(OTf)$_2$]. ESI-HRMS (CH_3CN) found: m/z = 1165.3267, calcd for $C_{66}H_{56}N_6O_5S^{64}ZnF_3^+$ = 1165.3276; IR (KBr): 3060, 1603, 1465, 1222, 1019, 768, 697, 634, 574 cm^{-1}; ^{1}H NMR (CD_3CN, δ): 8.80 (m, 1H), 7.54−7.19 (m, 40H), 3.79 (m, 2H), 3.54 (s, 3H), 3.26 (s, 3H), 1.10 (s, 6H).

[Zn(3−9−9)(OTf)$_2$]. ESI-HRMS (CH_3CN) found: m/z = 961.3076, calcd for $C_{50}H_{44}N_6O_5S^{64}ZnF_3^+$ = 961.2337; IR (KBr): 3063, 1615, 1295, 1165, 1019, 750, 701, 631, 574, 515 cm^{-1}; ^{1}H NMR (CD_3CN, δ): 7.51−7.32 (m, 20H), 7.12−7.13 (m, 4H), 6.98 (m, 4H), 3.92 (s, 3H), 3.69 (s, 3H), 3.30 (d, J = 3.3 Hz, 2H), 1.10 (s, 6H).

Job Plot Analysis. A 10 mM stock solution of the $LZn(OTf)_2$ complex [**Zn(2−6−6)(Otf)$_2$**] was prepared in 1.5 mL of CD_3OD; a 10 mM stock solution of *S*-TSA was prepared in 1.5 mL of CD_3OD. The NMR Job plot samples were prepared by combining the zinc complex and *S*-TSA stock solutions in the proportions 450 μL/50 μL, 350 μL/150 μL, 250 μL/250 μL, 150 μL/350 μL, 50 μL/450 μL, keeping the total concentration of L^{64}Zn(OTf)$_2$ plus *S*-TSA **13** constant at 10 mM. Samples were analyzed by ^{1}H NMR monitoring of the chemical shift (δ) of the imine proton signals as a function of the Zn/TSA ratio. The plots of $\Delta\delta \times [cat]^0$ versus $[cat]^0/([cat]^0 + [S\text{-}\mathbf{13}]^0)$ for [**Zn(2−6−6)(Otf)$_2$**] is given in Figure 6. A separate Job plot study was conducted as above for the *S*-substrate ester **1** in CD_3CN with the Zn-complex [**Zn(2−6−6)(OTf)$_2$**]. The Job plot graph showed an upward rise at 9:1 ratio of substrate to Zn.

Analysis of LZn(OTf)+ and LZn(TSA-13)+ Complexes by ESI-MS. Phase 1: Each building block (0.05 mmol of chiral diamine and 0.1 mmol of aldehydes) was dissolved in 4 mL of CH_3OH. Then 0.05 mmol of $Zn(OTf)_2$ was added to the above stirring mixture and the mixture allowed to equilibrate overnight at room temperature. Next, 100 μL of 0.05 mM solution of Bu_4NPF_6 in MeOH was added as an internal standard. A 220 μL stock solution A was prepared by pipetting 20 μL from the above library mixture and diluting it with 200 μL of CH_3OH. Then, 220 μL of a second stock solution (B) was prepared by pipetting 20 μL from stock solution A and diluting it with 200 μL of CH_3OH. Further, 20 μL of stock solution B was transferred into another vial and diluted with 200 μL of CH_3OH to obtain stock solution C. Solution C was screened by ESI-MS to detect the binary $[Zn(L)(OTf)_2]$ complex formation. Phase 2: To the above library aliquots, 1 mL of 0.05 mM of *S*-TSA or *R*-TSA **13** was added to form ternary complex libraries and kept stirring for 24 h at rt. ESI-MS samples were prepared by making different stock solutions (A, B, C) as described above and then the final solution C was taken for ESI-MS analysis, to monitor ternary $[LZn(\mathbf{13})]^+$ formation/amplification. Time dependent ternary [Zn(**2−4, −8, −10**)(TSA-**13**)] complex formation was monitored by the above procedure sampling at 2, 4.5, 27, and 35 min to establish attainment of equilibrium. The calculated relative abundance of the ternary complexes with enantiomeric *R*- and *S*-**13** = (ion count of peak/ion count of internal standard)/sum over all ions of (ion count of peak/ion count of internal standard). The ratio of these values for the enantiomeric **13** complexes is the stereoselectivity factor, α.

Similarly, experiments with pairs of aldehydes (**6**,**7**; **5**,**9**; **5**,**7**; **6**,**9**) showed their competitive ability to form ternary [Zn(L)TSA] complexes. ESI-MS analysis of library III (tetraphenyl-amine **3** + aldehydes (**4, 5, 6, 7, 8** and **9**) and $Zn(OTf)_2$) showed a variety of binary zinc complexes. Among 21 possibilities, 10 binary complexes were detected: $[^{64}Zn(3{-}4{-}5)(OTf)]^+$ (m/z = 889.2334), $[^{64}Zn(3{-}4{-}9)(OTf)]^+$ (m/z = 911.2174), $[^{64}Zn(3{-}5{-}5)(OTf)]^+$ (m/z = 917.2637), $[^{64}Zn(3{-}5{-}9)(OTf)^+$ (m/z = 939.2482), $[^{64}Zn(3{-}9{-}9)(OTf)]^+$ (m/z = 961.2335), $[^{64}Zn(3{-}9{-}7)(OTf)^+$ (m/z = 987.3320), $[^{64}Zn(3{-}7{-}7)(OTf)^+$ (m/z = 1013.2641), $[^{64}Zn(3{-}5{-}8)(OTf)^+$ (m/z = 1041.2956), $[^{64}Zn(3{-}8{-}9)(OTf)]^+$ (m/z = 1063.2803), $[^{64}Zn(3{-}7{-}8)(OTf)^+$ (m/z = 1089.2945). Attempts to template this library with *R*/*S*-TSA **13** in methanol resulted in rapid precipitation as was observed with CH_3CN, DMF, nitromethane, and isopropanol, as well with a lower amount of TSA **13** (LZn/TSA 1.0:0.1).

Analysis of Substrate Selectivity by ESI-MS. In a typical procedure 0.050 mmol of the diamine **2** or **3** and 0.10 mmol of *N*-*t*-butylimidazole carboxyaldehyde (**6**) were dissolved in 2 mL of dry CH_3CN and then 0.05 mmol of $Zn(OTf)_2$ was added and the resulting solution was stirred overnight at rt. Next, 100 μL of a 0.05 mM solution of Bu_4NPF_6 in CH_3CN was added as an internal standard. A 0.05 mM solution of (1 mL) of the *R*- or *S*-substrate **1** was then added to the above reaction mixture. After 1 h of stirring, a 220 μL stock solution (A) was prepared by pipetting 20 μL from the above reaction mixture and diluting it with 200 μL of CH_3CN. Then, 220 μL of a second stock solution (B) was prepared by pipetting 20 μL from stock solution A and diluting it with 200 μL of CH_3CN. Finally, 20 μL of stock solution B was pipetted out and diluted with 200 μL of CH_3CN to obtain stock solution C. Solution C was analyzed by ESI-MS to determine the formation of the substrate ternary complexes LZn(*R*- or *S*-**1**). Initially, we observed an ion at m/z = 641.1, calculated for $[^{64}Zn(\mathbf{2{-}6{-}6})(OTf)]^+$, $C_{24}H_{36}N_6O_5F_3S^{64}Zn^+$: 641.17. After adding the substrate **1** into the solution of binary complexes and stirring for 0.5 h at rt, ESI-MS analysis showed the appearance of a new set of peaks centered at m/z 359.7, calculated for $[(\mathbf{2{-}6{-}6})^{64}Zn(\mathbf{1})]^{2+}$, $C_{37}H_{49}N_7O_4{}^{64}Zn^{2+}/2$: 359.5.

Kinetics for Methanolysis of *R*- and *S*-Picolinate Ester (1) Catalyzed by Zn-Imine Complexes. The methanolysis of *R*- and *S*-1-phenylethanol picolinic acid ester (PEP, **1**) was carried out separately with the same substrate/catalyst concentrations; the reported rate constants (Table 3) are from single runs. A 10 mM stock solution of catalyst was prepared in 0.3 mL of CD_3OD/CD_2Cl_2 (1:1); 1.0 and 0.1 mM stock solutions of catalyst were prepared by serial dilutions of the stock solution with 1:1 CD_3OD/CD_2Cl_2. The samples for NMR reaction monitoring were prepared either from *R*- *or* *S*-ester (10 mM) by dissolving each into an NMR tube in 1 mL of CD_3OD/CD_2Cl_2 (1:1); then 100 μL of the catalyst solution (10 mM, 1.0 mM or 0.1 mM) was added. ^{1}H NMR spectra were recorded at two minute intervals (T = 292 K) while monitoring the disappearance of the substrate methyl signal at 1.95 ppm and the growth of the product alcohol methyl peak at 1.69 ppm. Initial rates were determined by plotting the peak integrals versus time (s) for the initial 10−20% conversion; the slopes of these plots divided by the initial concentrations of PEP (**1**) and the $LZn(OTf)_2$ complex provided the second order rate constants listed in Table 3.

■ ASSOCIATED CONTENT

Ⓢ Supporting Information

Synthesis of heterocyclic aldehydes and their characterization by ^{1}H, ^{13}C NMR, ESI-MS spectra of new compounds are given. The chiral diamines were synthesized using literature procedures and their spectral characterization is provided. ESI-MS spectra from selected library screenings are also given. This material is available free of charge via the Internet at http://pubs.acs.org.

dx.doi.org/10.1021/co3001023 | *ACS Comb. Sci.* 2013, 15, 90−100

AUTHOR INFORMATION

Corresponding Author

*Phone: 1-405-235-3696. Fax: 1-405-325-6111. E-mail: knicholas@ou.edu.

Funding

We are grateful for support of this project by the National Science Foundation.

Notes

The authors declare no competing financial interest.

ACKNOWLEDGMENTS

We thank Dr. Steven Foster (O.U. Mass Spectrometry Center) for assistance with the ESI-MS studies.

REFERENCES

(1) (a) Christianson, D. W.; Cox, J. D. Catalysis by metal-activated hydroxide in zinc and manganese metalloenzymes. *Annu. Rev. Biochem.* **1999**, *68*, 33−57. (b) Raup, D. E. A.; Cardinal-David, B.; Holte, D.; Scheidt, K. A. Cooperative catalysis by carbenes and Lewis acids in a highly stereoselective route to g-lactams. *Nature* **2010**, *21*, 766−771.

(2) (a) Strater, N.; Lipscomb, W. N.; Klabunde, T.; Krebs, B. Two-metal ion catalysis in enzymatic acyland phosphoryl-transfer reactions. *Angew. Chem., Int. Ed. Engl.* **1996**, *35*, 2024−2055. (b) Cacciapaglia, R.; Casnati, A.; Mandolini, L.; Reinhoudt, D. N.; Salvio, R.; Sartori, A.; Ungaro, R. Catalysis of diribonucleoside monophosphate cleavage by water soluble copper(II) complexes of calix[4]arene based nitrogen ligands. *J. Am. Chem. Soc.* **2006**, *128*, 12322−12330.

(3) (a) Matthews, B. W. Structural basis of the action of thermolysin and related zinc peptidases. *Acc. Chem. Res.* **1988**, *21*, 333−40. (b) Hofmann, T. *Top. Mol. Struct. Biol., 7* (Metalloproteins, Part 2) **1985**, 1−64.

(4) (a) Brown, R. S.; Neverov, A. A. Metal-catalyzed alcoholysis reactions of carboxylate and organophosphorus esters. *Adv. Phy. Org. Chem.* **2008**, *42*, 271−331. (b) Zhang, J.; Meng, X. G.; Zeng, X. C.; Yu, X. Q. Metallomicellar supramolecular systems and their applications in catalytic reactions. *Coord. Chem. Rev.* **2009**, *253*, 2166−2177. (c) Powell, A. K.; Deveson, A. C.; Collison, D.; Harper, D. R.; Mabbs, F. E. An investigation of the zinc sites of hydrolytic enzymes via a model compound approach. *Special Publications−R. Soc. Chem.* **1993**, *131*, 82−86. (d) Chin, J. Developing artificial hydrolytic metalloenzymes by a unified mechanistic approach. *Acc. Chem. Res.* **1991**, *24*, 145−52.

(5) (a) Vahrenkamp, H. Transitions, transition states, transition state analogues: Zinc pyrazolylborate chemistry related to zinc enzymes. *Acc. Chem. Res.* **1999**, *32*, 589−596. (b) Parkin, G. The bioinorganic chemistry of zinc: synthetic analogues of zinc enzymes that feature tripodal ligands. *Chem. Commun.* **2000**, 1971−1985. (c) Kimblin, C.; Allen, W. E.; Parkin, G. The synthesis and structure of $\{[Pim^{Pri,But}]ZnOH\}(ClO_4)$: Tris(imidazoly1)phosphine zinc hydroxide complex and a proposed structural model for carbonic anhydrase. *J. Chem. Soc., Chem. Commun.* **1995**, 1813−1815. (d) Kimblin, C.; Parkin, G. Comparison of zinc and cadmium coordination environments in synthetic analogues of carbonic anhydrase: Synthesis and structure of $\{[Pim^{Pri,But}]Cd(OH_2)(OClO_3)\}(ClO_4)$. *Inorg. Chem* **1996**, *35*, 6912−6913.

(6) Dro, C.; Bellemin-Laponnaz, S.; Welter, R.; Gade, L. H. A C3-symmetrical chiral trisoxazoline zinc complex as a functional model for zinc hydrolases: Kinetic resolution of racemic chiral esters by transesterification. *Angew. Chem., Int. Ed.* **2004**, *43*, 4479−4482.

(7) (a) Fife, T. H.; Przystas, T. J. Divalent metal ion catalysis in the hydrolysis of esters of picolinic acid. Metal ion promoted hydroxide ion and water catalyzed reactions. *J. Am. Chem. Soc.* **1985**, *107*, 1041−1047. (b) Qiu, L. G.; Jiang, X.; Gu, L. N.; Hu, G. Gemini metallomicellar catalysis: Hydrolysis of p-nitrophenylpicolinate catalyzed by Cu(II) and Ni(II) complexes of macrocyclic ligands in gemini surfactant micelles. *J. Mol. Catal. A: Chem.* **2007**, *277*, 15−20. (c) Cheng, S. Q. Kinetics and mechanism of metal cation catalysis in the hydrolysis of p-nitrophenyl picolinate (PNPP). *Pol. J. Chem.* **2005**, *79*, 933−939.

(8) Matsumoto, M.; Estes, D.; Nicholas, K. M. Evolution of metal complex-catalysts by dynamic templating with transition state analogs. *Eur. J. Inorg. Chem.* **2010**, 1847−1852.

(9) (a) Pauling, L. Chemical achievement and hope for the future. *Am. Sci.* **1948**, *36*, 51−58. (b) Jencks, W. P. *Catalysis in Chemistry and Enzymology*; McGraw-Hill: New York, 1969.

(10) (a) Kagan, H. B.; Fiaud, J. C. Kinetic resolution. *Top. Stereochem.* **1988**, *18*, 249. (b) Williams, J. M. J.; Parker, R. J.; Neri, C. Enzymatic kinetic resolution. In *Enzyme Catalysis in Organic Synthesis*; Drauz, K., Waldman, H., Eds.; Wiley-VCH: Weinheim, Germany, 2002; Vol. *1*, pp 287−312.

(11) Tokunaga, M.; Aoyama, H.; Kiyosu, J.; Shirogane, Y.; Iwasawa, T.; Obora, Y.; Tsuji, Y. Metal complexes-catalyzed hydrolysis and alcoholysis of organic substrates and their application to kinetic resolution. *J. Organomet. Chem.* **2007**, *692*, 472−480.

(12) Yoon, P. T.; Jacobsen, E. N. Privileged chiral catalysts. *Science* **2003**, *299*, 1691−1693.

(13) Maxwell, C. I.; Shah, K.; Samuleev, P. V.; Neverov, A. A.; Brown, R. S. Kinetic resolution of esters via metal catalyzed methanolysis reactions. *Org. Biomol. Chem.* **2008**, *6*, 2796−2803.

(14) Baek, J. Y.; Shin, Y. J.; Jeon, H. B.; Kim, K. S. Picolinyl group as an efficient alcohol protecting group: cleavage with $Zn(OAc)_2.2H_2O$ under a neutral condition. *Tetrahedron Lett.* **2005**, *46*, 5143−5147.

(15) Sammakia, T.; Jacobs, J. S. Picolinic Acid as a Partner in the Mitsunobu reaction: subsequent hydrolysis of picolinate esters under essentially neutral conditions with copper acetate in methanol. *Tetrahedron Lett.* **1999**, *40*, 2685−2688.

(16) Kannappan, R.; Matsumato, M.; Hallren, J.; Nicholas, K. M. New chiral Schiff base-zinc complexes and their esterolytic catalytic activity. *J. Mol. Catal. A: Chem.* **2011**, *339*, 72−78.

(17) Brodbelt, J. S. Probing molecular recognition by mass spectrometry. *Int. J. Mass Spectrom.* **2000**, *200*, 57−69.

(18) Brodbelt, J. S. Evaluation of DNA/ligand interactions by electrospray ionization mass spectrometry. *Annu. Rev. Anal. Chem.* **2010**, *3*, 67−87.

(19) Chow, C.-F.; Fuji, S.; Lehn, J. M. Metallodynamers: Neutral dynamic metallosupramolecular polymers displaying transformation of mechanical and optical properties on constitutional exchange. *Angew. Chem., Int. Ed.* **2007**, *46*, 5007−5010.

(20) Schroeder, D. Applications of electrospray ionization mass spectrometry in mechanistic studies and catalysis research. *Acc. Chem. Res.* **2012**, *45*, 1521−1532.

(21) Marquis-Rigault, A.; Dupont-Gervais, A.; Baxter, P. N. W.; Dorsselaer, A. V.; Lehn, J.-M. Self-assembly of an 11-component cylindrical inorganic architecture: Electrospray mass spectrometry and thermodynamic studies. *Inorg. Chem.* **1996**, *35*, 2307−2310.

(22) Prema, D.; Wyznicia, A. V.; Scott, B.; Hilborn, J.; Desper, J.; Levy, C. Dinuclear zinc(II) complexes of symmetric Schiff-base ligands with extended quinoline sidearms. *Dalton Trans.* **2007**, 4788−4796.

(23) Sterk, D.; Stephan, M. S.; Mohar, B. New chiral N-(N,N-dialkylamino)sulfamoyl-1,2-diamine ligands for highly enantioselective transfer hydrogenation of ketones. *Tetrahedron: Asymmetry* **2002**, *13*, 2605−2608.

(24) Ng, K.; Somanathan, R.; Walsh, P. J. Synthesis of homochiral pentadentate sulfonamide-based ligands. *Tetrahedron: Asymmetry* **2001**, *12*, 1719−1722.

(25) (a) Liang, J. Y., Lipscomb, W. N. In *Proceedings of the International Workshop on Carbonic Anhydrase*, Spoleto, Italy, 1991; VCH: Weinheim, Germany, **1991**; pp 50−64. (b) Remko, M. Molecular structure, pKa, lipophilicity, solubility and absorption of biologically active aromatic and heterocyclic sulfonamides. *J. Mol. Struct. THEOCHEM.* **2010**, *944*, 34−42.

(26) Obreza, A.; Gobec, S. Recent advances in design, synthesis and biological activity of aminoalkylsulfonates and sulfonamidopeptides. *Curr. Med. Chem.* **2004**, *11*, 3263−78.

(27) Seebach, D.; Pichota, A.; Beck, A. K.; Pinkerton, A. B.; Litz, T.; Karjalainen, J.; Gramlich, V. Preparation of TADDOL derivatives for new applications. *Org. Lett.* **1999**, *1*, 55−58.
(28) Nindakova, L. O.; Shainyan, B. A.; Badyrova, N. M.; Lebed, F. M. Asymmetric hydrogen-transfer hydrogenation on rhodium(I)-complexes with new optically active salen ligands derived from (4S,5S)-4,5-Bis(aminomethyl)-2,2-dimethyl-1,3-dioxolane. *Russ. J. Org. Chem.* **2012**, *48*, 59−63.
(29) Nindakova, L. O.; Lebed, F. M.; Zamazei, A. Y.; Shainyan, B. A. New C2-symmetric optically active salen ligands and their cobalt(II) complexes. Hydridoborate reduction of prochiral C═O and C═C bonds. *Russ. J. Org. Chem.* **2007**, *43*, 1322−1329.
(30) Gan, G. Asymmetric nitroaldol reaction with a chiral copper complex derived from D-tartaric acid. *Can. J. Chem.* **2008**, *86*, 261−263.
(31) Related N_4-tetradentate-Zn complexes have K_f = 10^8-10^{11}: Liang, J.; Zhang, J.; Zhu, L.; Duarandin, A.; Young, V. G., Jr.; Geacintov, N.; Canary, J. W. Structures, Metal Ion Affinities, and Fluorescence Properties of Soluble Derivatives of Tris((6-phenyl-2-pyridyl)methyl)amine. *Inorg. Chem.* **2009**, *48*, 11196−11208.
(32) Berreau, L. M. Bioinorganic chemistry of group 12 complexes supported by tetradentate tripodal ligands having internal hydrogen-bond donors. *Eur. J. Inorg. Chem.* **2006**, 273−283.
(33) Loran, J. S.; Naylor, R. A.; Williams, A. J. Direct N-methylation of 2-pyridylphosphonic acids by diazomethane. *J. Chem. Soc., Perkin Trans. 2* **1976**, 1444−1447.
(34) Mock, W. L.; Cheng, H. Principles of hydroxamate inhibition of metalloproteases: Carboxypeptidase A. *Biochemistry* **2000**, *39*, 13945−13952.
(35) John, G. J. W.; Arie, K.; Johan, F. J. E. Carboxylic and phosphate ester hydrolysis catalysed by bivalent zinc and copper metallosurfactants. *J. Chem. Soc., Perkin Trans.* **1991**, *2*, 1121−1126.
(36) Zn(**13**)$_2$ has been prepared and structurally characterized , Estes, D.; Matsumoto, S.; Powell, D.; Nicholas, K. M. unpublished results, 2010; see also Fry, J. A.; Samanamu, C. R.; Montchamp, J.-L.; Richards, A. F. A mild synthetic route to zinc, cadmium, and silver polymers with (2-Pyridyl)phosphonic Acid: Synthesis and analysis. *Eur. J. Inorg. Chem.* **2008**, 463−470.
(37) McNeil, S. W.; DuMez, D. D.; Matano, Y.; Lovell, S.; Mayer, J. M. Synthesis and reactivity of aryl- and alkyl-rhenium(V)imido-triflate compounds: An unusual mechanism for triflate substitution. *Organometallics* **1999**, *18*, 3715−3727.
(38) pK_a - Acidity constants, Williams, R.; Jencks, W. P.; and Westheimer, F. H.; , http://www.webqc.org/pkaconstants.php.
(39) Maxwell, C. I.; Shah, K.; Samuleev, P. V.; Neverov, A. A.; Brown, R. S. Kinetic resolution of esters via metal catalyzed methanolysis reactions. *Org. Biomol. Chem.* **2008**, *6*, 2796−2803.
(40) Wassenaar, J.; Jansen, E.; Jan van Zeist, W.; Bickelhaupt, F. M.; Siegler, M. A.; Spek, A. L.; Reek, J. N. H. Catalyst selection based on intermediate stability measured by mass spectrometry. *Nature* **2010**, *2*, 417−421.
(41) Bodanszky, M.; du Vigneaud, V. Synthesis of a biologically active analog of oxytocin, with phenylalanine replacing tyrosine. *J. Am. Chem. Soc.* **1959**, *81*, 6072−6075.
(42) Hilgraf, R.; Pfaltz, A. Chiral Bis(*N*-sulfonylamino)phosphine- and TADDOL-phosphite-oxazoline ligands: Synthesis and application in asymmetric catalysis. *Adv. Synth. Cat.* **2005**, *347*, 61−77.
(43) LaRonde, F. J.; Brook, M. A. Stereoselective reduction of ketones using extracoordinate silicon: C2-symmetric ligands. *Inorg. Chim. Acta* **1999**, *296*, 208−221.
(44) Sauerbrey, S.; Majhi, P. K.; Daniels, J.; Schnakenburg, G.; Brandle, G. M.; Scherer, K.; Streubel, R. Synthesis, Structure, and Reactions of 1-tert-Butyl-2-diphenylphosphino-imidazole. *Inorg. Chem.* **2011**, *50*, 793−799.
(45) Katritzky, A. R.; He, H. -Y.; Long, Q.; Cui, X.; Level, J.; Wilcox, A. L. The preparation of some heteroaromatic and aromatic aldehydes. *ARKIVOC* **2000**, 240−251.